mathematics

MDPI

Article

Dynamical Behavior of Solitary Waves for the Space-Fractional Stochastic Regularized Long Wave Equation via Two Distinct Approaches

Muneerah Al Nuwairan *, Bashayr Almutairi and Anwar Aldhafeeri

Department of Mathematics and Statistics, College of Science, King Faisal University, P.O. Box 400, Al-Ahsa 31982, Saudi Arabia; 222400521@student.kfu.edu.sa (B.A.); aaaldhafeeri@kfu.edu.sa (A.A.)
* Correspondence: msalnuwairan@kfu.edu.sa

Abstract

This study investigates the influence of multiplicative noise—modeled by a Wiener process—and spatial-fractional derivatives on the dynamics of the space-fractional stochastic Regularized Long Wave equation. By employing a complete discriminant polynomial system, we derive novel classes of fractional stochastic solutions that capture the complex interplay between stochasticity and nonlocality. Additionally, the variational principle, derived by He's semi-inverse method, is utilized, yielding additional exact solutions that are bright solitons, bright-like solitons, kinky bright solitons, and periodic structures. Graphical analyses are presented to clarify how variations in the fractional order and noise intensity affect essential solution features, such as amplitude, width, and smoothness, offering deeper insight into the behavior of such nonlinear stochastic systems.

Keywords: stochastic fractional differential equations; variational principle; semi inverse method; complete discriminate system; long wave equation; modified Riemann–Liouville derivative

MSC: 34A08; 34K50; 37H10



Academic Editor: Nikolaos L. Tsitsas

Received: 15 June 2025
Revised: 1 July 2025
Accepted: 3 July 2025
Published: 4 July 2025

Citation: Al Nuwairan, M.; Almutairi, B.; Aldhafeeri, A. Dynamical Behavior of Solitary Waves for the Space-Fractional Stochastic Regularized Long Wave Equation via Two Distinct Approaches. *Mathematics* **2025**, *13*, 2193. https://doi.org/10.3390/math13132193

Copyright: © 2025 by the authors. Licensee MDPI, Basel, Switzerland. This article is an open access article distributed under the terms and conditions of the Creative Commons Attribution (CC BY) license (https://creativecommons.org/licenses/by/4.0/).

1. Introduction

Partial differential equations (PDEs) are used in describing dynamic processes in physical, biological, and financial systems [1,2]. Traditional PDEs are deterministic, yet many natural and engineered systems exhibit inherent randomness due to factors such as environmental noise, measurement inaccuracies, and unpredictable disturbances. To account for such uncertainties, Stochastic Partial Differential Equations (SPDEs) are used. These equations integrate stochastic components—often as random noise or probabilistic forcing terms—into the classical PDEs [3]. SPDEs find applications in domains where uncertainty significantly influences outcomes, including turbulence modeling, neural activity analysis, quantitative finance, and climate prediction [4–13]. The study of SPDEs merges techniques from functional analysis, probability theory, and stochastic calculus, creating a vibrant, interdisciplinary field. However, many real-world phenomena exhibit memory effects and anomalous diffusion, which cannot be adequately captured by classical SPDEs. This limitation has led to the development of Fractional Stochastic Partial Differential Equations (FSPDEs), which incorporate fractional derivatives to account for long-range dependencies and nonlocal interactions [14].

The long wave equation is a mathematical framework for inspecting shallow-water dynamics, particularly in systems where waves exhibit weak nonlinearity and dispersion. This model captures the behavior of long-wave propagation and has been applied to simulate various natural phenomena. Initially proposed by Peregrine [15] to describe undular bore formation, the equation was later extended in [16] to derive the Korteweg–de Vries (KdV) equation, which models small-amplitude, long-wavelength one-dimensional surface gravity waves. Further refinements led to the Regularized Long Wave (RLW) equation, which includes regularization terms to improve wave dispersion modeling and propagation accuracy [16]. Mathematically, the RLW equation is defined as follows:

$$\mathcal{H}_t + \mathcal{H}_x - \frac{r}{2}\mathcal{H}\mathcal{H}_x - s\mathcal{H}_{xxt} = 0. \tag{1}$$

The parameters r and s are constants that govern the nonlinear and dispersive properties of the system. The function $\mathcal{H}(x,t)$ denotes the wave amplitude, where x and t represent the spatial and temporal coordinates, respectively.

Depending on the constraints imposed on the constants r and s, Equation (1) can be utilized to model various physical phenomena, including dissipative processes in heat conduction, ion-acoustic plasma waves, and nonlinear wave diffusion. The parameters r and s govern the behavior of the RLW equation. For instance, when $r = 0$ and $s = 0$, Equation (1) reduces to a linear wave equation, which describes wave propagation with small amplitudes. When $r > 0$ and $s = 1$, the equation exhibits nonlinearity, with the wave's amplitude varying during propagation. For $s > 1$, dispersive effects emerge, enabling the wave to alter its shape as it travels as a result of frequency-dependent variations in wave velocity. Numerous analytical and numerical techniques have been employed to solve Equation (1) [17–20]. Notably, soliton solutions can arise from the interplay between the final two terms, maintaining a balance that preserves the wave structure.

The RLW equation has undergone various modifications through the incorporation of fractional derivatives, broadening its applicability across different contexts. Researchers have examined approaches to solving these generalized versions, resulting in advances in both analytical techniques and numerical methods [21–23].

This study introduces an extended formulation of the RLW Equation (1), incorporating Jumarie's modified Riemann–Liouville fractional derivative [24] and a stochastic component [25]. The generalized equation is given by the following:

$$\mathrm{d}\mathcal{H} + [\mathbb{D}_x^p\mathcal{H} - \frac{r}{2}\mathcal{H}\mathbb{D}_x^p\mathcal{H}]\mathrm{d}t - s\mathbb{D}_x^{2p}\mathrm{d}\mathcal{H} = \sigma(\mathcal{H} - s\mathbb{D}_x^{2p}\mathcal{H})\mathrm{d}\mathbb{B}, \tag{2}$$

where $\mathbb{D}^p$ is the Jumarie's modified Riemann–Liouville fractional derivative of order p (JRLD), σ is the noise strength, $\mathbb{B}(t)$ is a white noise (Gaussian process), and $\mathcal{H}\mathrm{d}\mathbb{B}$ is a multiplicative white noise in the Itô sense. It should be noted that the noise term is a combination of the two terms appearing in [26,27]. We chose a standard Wiener process to model the noise since it enables analytical solutions and qualitative insights into stochastic-nonlocal interactions. Equation (2) was first introduced in our study [28], where the bifurcation method was employed to generate novel solutions and to analyze the individual effects of fractional-order derivatives and noise intensity. The authors in [29] refined the auxiliary function method, applying it to obtain new solutions and examine the impact of fractional derivatives and noise strength on the results. The deterministic form of Equation (2), corresponding to the integer-order derivatives ($\sigma = 0, p = 1$), has been studied by several researchers [30–32]. The Saint-Venant-type models—such as those introduced by Peregrine [33] and later extended by Shi et al. [34], Chazel et al. [35], and Popinet [36]—provide a more comprehensive description of geophysical flows by describing both wave amplitude and momentum. In contrast, the one-equation RLW

model, which we use in our study, primarily focuses on wave amplitude and does not fully account for the evolution of momentum. This limitation on the descriptive power of our model is compensated for by the ability to analytically treat the stochastic and factional aspects of the model.

A fundamental challenge in the study of FSPDEs is finding their analytical solutions, which are important in understanding and interpreting the underlying phenomena. The current study aims to obtain new solutions to Equation (2) for all possible values of the two parameters r and s, employing two reliable approaches: the complete discriminant polynomial system [37] and He's variational method [38]. In addition, we investigate the influence of the fractional derivative order and the standard Wiener process on the obtained solutions.

The structure of this paper is as follows: Section 1 presents the reduction of the SFRLW Equation (2) to an equivalent ordinary differential equation. In Section 3, we apply the complete discriminant polynomial system to determine the intervals of real propagation, identify bounded and physically relevant non-complex solutions, and construct new solutions for the SFRLW equation. In Section 4, we use He's variational method to derive additional solutions, classified as bright solitons, bright-like solitons, kinky bright solitons, and periodic solutions. Section 5 graphically illustrates the effect of the fractional derivative order and noise strength on the obtained solutions. Finally, Section 6 provides a summary of the results.

2. Wave Solutions

To determine a solution for Equation (2), we consider solutions that have the following form:

$$\mathcal{H}(x,t) = N(\xi)e^{\sigma\mathbb{B}(t)-\frac{\sigma^2}{2}t}, \qquad \xi = \frac{kx^p}{\Gamma(p+1)} + \omega t, \tag{3}$$

where ω and k are free parameters, and $\Gamma(\cdot)$ is the Gamma function [39]. Using direct computation, we obtain

$$\mathrm{d}\mathcal{H} = e^{\sigma\mathbb{B}(t)-\frac{\sigma^2}{2}t}[\omega N'\mathrm{d}t + N(\rho\mathrm{d}\mathbb{B} + \frac{\sigma^2}{2} - \frac{\sigma^2}{2})], \tag{4a}$$

$$\mathbb{D}_x^p\mathcal{H} = ke^{\sigma\mathbb{B}(t)-\frac{\sigma^2}{2}t}N', \tag{4b}$$

$$\mathbb{D}_x^{2p}\mathcal{H} = k^2e^{\sigma\mathbb{B}(t)-\frac{\sigma^2}{2}t}N'', \tag{4c}$$

$$\mathbb{D}_x^{2p}\mathrm{d}\mathcal{H} = k^2[\omega N'''\mathrm{d}t + \sigma N''\mathrm{d}\mathbb{B}]e^{\sigma\mathbb{B}(t)-\frac{\sigma^2}{2}t}, \tag{4d}$$

where $'$ denotes differentiation with respect to ξ, and $+\frac{\rho^2}{2}N$ is the Itô correction term. Substituting the expressions (4) into Equation (2), we obtain

$$-n\omega k^2N''' - \frac{mk}{2}NN'e^{\sigma\mathbb{B}(t)}e^{-\frac{\sigma^2}{2}t} + (\omega+k)N' = 0. \tag{5}$$

Since $\mathbb{B}(t)$ follows a normal distribution, the expectation satisfies $\mathbb{E}(e^{\sigma\mathbb{B}(t)}) = e^{\frac{\sigma^2}{2}t}$ (see [25] for details). Taking the expectations of both sides of Equation (5), we obtain

$$N''' + \frac{r}{2sk\omega}NN' - \frac{\omega+k}{2sk^2\omega}N' = 0, \tag{6}$$

integrating Equation (6) gives

$$N'' + \frac{r}{4sk\omega}N^2 - \frac{\omega+k}{s\omega\,k^2}N + c_1 = 0, \tag{7}$$

where c_1 is the integration constant. Multiplying both sides of Equation (7) by N' and integrating the resultant equation, we obtain

$$\frac{1}{2}N'^2 + \frac{r}{12sk\omega}N^3 - \frac{\omega+k}{2k^2s\omega}N^2 + c_1N + c_2 = 0. \tag{8}$$

where c_2 is the integration constant.

Thus, the problem of solving Equation (2) reduces to determining $N(\xi)$, which satisfies Equation (8). To accomplish this, we use two distinct analytical approaches: first, the complete discriminant method is utilized to derive novel solutions; second, He's variational method is employed to generate additional exact solutions, thereby expanding the solution family of Equation (2).

3. Complete Discriminate Method

The complete discrimination system for polynomials generalizes the classical discriminant $\Delta = a_1^2 - 4a_1a_2$ for quadratic polynomials $x^2 + a_1x + a_2$, but the calculation of the complete discriminant increases in complexity for polynomials of higher degree. Yang et al. developed an algorithmic solution using computer algebra programs, enabling the systematic computation of complete discrimination systems for polynomials [37]. This method has since been successfully applied in various studies, including [40].

To simplify the computations, we translate the origin, $N \to \mathcal{A} + \frac{2(\omega+k)}{rk}$ so, Equation (8) becomes

$$\frac{1}{2}\mathcal{A}'^2 - \alpha(\mathcal{A}^3 + \beta\mathcal{A} + \delta) = 0, \tag{9}$$

where α, β, and δ are constants whose values are

$$\begin{aligned} \alpha &= -\frac{r}{12sk\omega}, \qquad \beta = \frac{12\left(c_1rs\omega\, k^3 - k^2 - 2\omega k - \omega^2\right)}{r\, k^2 r}, \\ \gamma &= \frac{12sk\omega}{r}\left(-\frac{4(\omega+k)^3}{3r^2s\omega\, k^4} + \frac{2c_1(\omega+k)}{kr} + c_2\right). \end{aligned} \tag{10}$$

Separating the variables in Equation (10) yields the one differential form

$$\frac{\mathrm{d}\mathcal{A}}{\sqrt{F_3(\mathcal{A})}} = \pm\sqrt{2}\mathrm{d}\xi, \tag{11}$$

where the cubic polynomial $F_3(\mathcal{A})$ is given by

$$F_3(\mathcal{A}) = \mathcal{A}^3 + \beta\mathcal{A} + \gamma. \tag{12}$$

Integrating both sides of Equation (11) requires determining the range of the included parameters α, β, and γ. This range can be computed by using the complete discriminant polynomial system for the polynomial (12), which takes the form

$$\Delta = -\left(\frac{\gamma^2}{4} + \frac{\beta^3}{27}\right). \tag{13}$$

By applying the complete discrimination system (13), we identify four distinct cases that require analysis using the polynomial method.

Case A. If $\Delta = 0$ and $\beta < 0$, the polynomial (12) has a simple root, ψ_1, and a double root, $-2\psi_1$, where $\psi_1 > 0$. Consequently, it can be expressed as $F_3(\mathcal{A}) = (\mathcal{A} - \psi_1)^2(\mathcal{A} + 2\psi_1)$. Two distinct solutions to Equation (11), arise depending on whether α is positive or negative.

I. If $\alpha > 0$, then the intervals of the real solutions are $(-2\psi_1, \psi_1)$ and (ψ_1, ∞). By assuming $\mathcal{A} \in (-2\psi_1, \psi_1)$, we integrate (11) with assumption that $\mathcal{A}(0) = -2\psi_1$ to derive a solution to Equation (6) and subsequently to the main equation of the form

$$\mathcal{H}(x,t) = \left[-2\psi_1 + \frac{2(\omega+k)}{rk} + 3\psi_1 \tanh^2\left(\sqrt{\frac{3\alpha\psi_1}{2}}\left(\frac{kx^p}{\Gamma(p+1)} + \omega t\right)\right)\right] e^{\sigma\mathbb{B}(t) - \frac{\sigma^2}{2}t}, \quad (14)$$

The solution (14) is a new solution to Equation (2). On the other hand, if we use the interval (ψ_1, ∞), then the integration of Equation (11) with the condition $\mathcal{A}(0) = \psi_1$ gives

$$\mathcal{H}(x,t) = \left[-2\psi_1 + \frac{2(\omega+k)}{rk} + 3\psi_1 \coth^2\left(\coth^{-1}\left(\frac{\pi}{4}\right) \mp \sqrt{\frac{3\alpha\psi_1}{2}}\left(\frac{kx^p}{\Gamma(p+1)} + \omega t\right)\right)\right] e^{\sigma\mathbb{B}(t) - \frac{\sigma^2}{2}t}, \quad (15)$$

which is a novel solution to Equation (2).

II. If $\alpha < 0$, then $(-\infty, -2\psi_1)$ is the only interval of real solutions. To obtain a solution for Equation (2), we integrate Equation (11), yielding the expression:

$$\mathcal{H}(x,t) = \left[-2\psi_1 + \frac{2(\omega+k)}{rk} - 3\psi_1 \tan^2\left(\sqrt{\frac{-3\alpha\psi_1}{2}}\left(\frac{kx^p}{\Gamma(p+1)} + \omega t\right)\right)\right] e^{\sigma\mathbb{B}(t) - \frac{\sigma^2}{2}t}, \quad (16)$$

This is a novel solution to Equation (2).

Case B. If $\Delta = 0$ and $\beta = 0$, then the polynomial (12) has one real root at the origin of multiplicity three and thus $F_3(\mathcal{A}) = \mathcal{A}^3$. Thus, we have the following cases:

I. If $\alpha > 0$, the interval of the real solution is $(0, \infty)$. We integrate both sides of Equation (11) with assumption $\mathcal{A}(0) = \infty$ to obtain

$$\mathcal{H}(x,t) = \left[\frac{2(\omega+k)}{rk} + \frac{1}{\frac{\alpha}{2}\left(\frac{kx^p}{\Gamma(p+1)} + \omega t\right)^2}\right] e^{\sigma\mathbb{B}(t) - \frac{\sigma^2}{2}t}. \quad (17)$$

II. If $\alpha < 0$, the interval of real solutions is $(-\infty, 0)$. Assuming $\mathcal{A}(0) = -\infty$ and integrating both sides of Equation (11), we obtain

$$\mathcal{H}(x,t) = \left[\frac{2(\omega+k)}{rk} - \frac{1}{\frac{\alpha}{2}\left(\frac{kx^p}{\Gamma(p+1)} + \omega t\right)^2}\right] e^{\sigma\mathbb{B}(t) - \frac{\sigma^2}{2}t}. \quad (18)$$

Case C. If $\Delta > 0$ and $\beta < 0$, then the polynomial (12) has three real roots denoted by ψ_2, ψ_3, and ψ_4 with $\sum_{j=2}^{4} \psi_j = 0$ and ordered as $\psi_2 < \psi_3 < \psi_4$. Thus, the polynomial (12) can be expressed as $F_3 = (\mathcal{A} - \psi_2)(\mathcal{A} - \psi_3)(\mathcal{A} - \psi_4)$. Subsequent computations depend on the sign α as follows

I. If $\alpha > 0$, then we will have real solutions to Equation (2) when $\mathcal{A} \in (\psi_2, \psi_3) \cup (\psi_4, \infty)$. If $\mathcal{A} \in (\psi_2, \psi_3)$, we integrate both sides of Equation (11) assuming $\mathcal{A}(0) = \psi_2$ to obtain

$$\mathcal{H}(x,t) = \left[\psi_2 + \frac{2(\omega+k)}{rk} + (\psi_3 - \psi_2)\mathrm{sn}^2\left(\sqrt{\frac{\alpha}{2}(\psi_4 - \psi_2)}\left(\frac{kx^p}{\Gamma(p+1)} + \omega t\right), \sqrt{\frac{\psi_3 - \psi_2}{\psi_4 - \psi_2}}\right)\right] \times e^{\sigma\mathbb{B}(t) - \frac{\sigma^2}{2}t}, \quad (19)$$

where $\mathrm{sn}(u,k)$ is a Jacobi elliptic function [41]. The solution (19) is a new solution to Equation (2). On the other hand, if we assume $\mathcal{A} \in (\psi_4, \infty)$, the integration of Equation (11) yields

$$\mathcal{H}(x,t) = \left[\psi_3 + \frac{2(\omega+k)}{rk} + (\psi_4-\psi_3)\mathrm{ns}^2\left(\sqrt{\frac{\alpha}{2}(\psi_4-\psi_2)}\left(\frac{kx^p}{\Gamma(p+1)}+\omega t\right), \sqrt{\frac{\psi_3-\psi_2}{\psi_4-\psi_2}}\right)\right] \times e^{\sigma\mathbb{B}(t)-\frac{\sigma^2}{2}t}, \tag{20}$$

where $\mathrm{ns}(u,k) = 1/\mathrm{sn}(u,k)$ is an elliptic function [41]. The solution (20) is novel solution to Equation (2).

II. If $\alpha < 0$, the intervals, yielding real solutions to Equation (2), are $(-\infty, \psi_2)$ and $\cup(\psi_3, \psi_4)$. Assuming $\mathcal{A} \in (\psi_3, \psi_4)$ and integrating both sides of Equation (11) with $\mathcal{A}(0) = \psi_2$ gives

$$\mathcal{H}(x,t) = = \left[\psi_4 + \frac{2(\omega+k)}{rk} - (\psi_4-\psi_3)\mathrm{sn}^2\left(\sqrt{\frac{-\alpha}{2}(\psi_4-\psi_2)}\left(\frac{kx^p}{\Gamma(p+1)}+\omega t\right), \sqrt{\frac{\psi_3-\psi_2}{\psi_4-\psi_2}}\right)\right] \times e^{\sigma\mathbb{B}(t)-\frac{\sigma^2}{2}t}, \tag{21}$$

which is a novel solution of Equation (2). If we assume $\mathcal{A} \in (-\infty, \psi_2)$, and integrate Equation (11) with $\mathcal{A}(0) = \psi_2$, then

$$\mathcal{H}(x,t) = \left[\psi_3 + \frac{2(\omega+k)}{rk} - (\psi_3-\psi_2)\mathrm{sn}^2\left(\sqrt{\frac{-\alpha}{2}(\psi_4-\psi_2)}\left(\frac{kx^p}{\Gamma(p+1)}+\omega t\right), \sqrt{\frac{\psi_3-\psi_2}{\psi_4-\psi_2}}\right)\right] \times e^{\sigma\mathbb{B}(t)-\frac{\sigma^2}{2}t}. \tag{22}$$

Case D. If $\Delta < 0$, then the polynomial (12) has a single real root, denoted as ψ_5, along with a pair of complex conjugate roots, denoted by ψ_6 and ψ_6^*, where * indicates complex conjugate. Thus, it can be expressed as follows: $F_3(\mathcal{A}) = (\mathcal{A}-\psi_5)(\mathcal{A}-\psi_6)(\mathcal{A}-\psi_6^*)$. Further computations depend on the sign of α. Accordingly, we examine the two possible cases separately.

I. When $\alpha > 0$, the real solution to Equation (2) exists for $\mathcal{A} \in (\psi_5, \infty)$. We integrate both sides of Equation (11) with postulating $\mathcal{A}(0) = \psi_5$. To obtain a new solution to Equation (2) of the form

$$\mathcal{H} = \left[\psi_5 - B + \frac{2(\omega+k)}{rk} + \frac{2B}{1+\mathrm{cn}(\sqrt{2\alpha\, B}(\frac{kx^p}{\Gamma(p+1)}+\omega t), \kappa_1)}\right] \times e^{\sigma\mathbb{B}(t)-\frac{\sigma^2}{2}t}, \tag{23}$$

where $B^2 = \frac{9}{4}\psi_5^2 + \mathrm{Im}^2\psi_6$ and $\kappa_1^2 = \frac{2B-3\psi_5}{4B}$.

II. For $\alpha < 0$, Equation (2) has a periodic solution if $\mathcal{A} \in (-\infty, \psi_5)$. We integrate both sides of Equation (11) with assumption $\mathcal{A}(0) = \psi_5$ to obtain

$$\mathcal{H} = \left[\psi_5 + B + \frac{2(\omega+k)}{rk} - \frac{2B}{1+\mathrm{cn}(\sqrt{-2\alpha\, B}(\frac{kx^p}{\Gamma(p+1)}+\omega t), \kappa_2)}\right] \times e^{\sigma\mathbb{B}(t)-\frac{\sigma^2}{2}t},$$

where $\kappa_2^2 = \frac{2B+3\psi_5}{4B}$. The solution (24) is novel solution to Equation (2).

It is worth noting that the concept of intervals in real wave propagation is significant, since identical parameter conditions can lead to distinct types of solutions. To illustrate this, consider the case where $\Delta > 0$, $\beta < 0$, and $\alpha > 0$. Under these conditions, we obtain two different solutions, (19) and (20), each corresponding to a different interval of real

wave propagation. The solution (19) exhibits periodic behavior, whereas the solution (20) is unbounded. Therefore, the intervals of real wave propagation cannot be overlooked.

4. Variational Principle

To derive the variational principle for the solution, we employ the semi-inverse method [42,43], a well-established technique for constructing variational formulations. This approach involves introducing an undetermined function as a trial functional [44,45]. We utilize this to develop the variational principle for Equation (7).

$$\mathcal{J} = \int \left[-\frac{1}{2} N'^2(\xi) + \frac{r}{12sk\omega} N(\xi)^3 - \frac{\omega + k}{2k^2 s\omega} N(\xi)^2 + c_1 N(\xi) \right] \mathrm{d}\xi. \tag{24}$$

A direct comparison between Equations (7) and (24) shows that the variational principle has reduced the order of Equation (7). This plays a crucial role in our subsequent derivation of soliton and periodic solutions for Equation (2).

4.1. Bright Soliton

Following He's variational method, we will assume that the bright soliton of Equation (2) has the form as [46,47]:

$$N(\xi) = N_1 \mathrm{sech}(\xi), \tag{25}$$

where N_1 is a constant. Substituting Equation (25) into Equation (24), we obtain

$$\begin{aligned} \mathcal{J}(N_1) &= \int_0^\infty \left[-\frac{1}{2} N'^2(\xi) + \frac{r}{12sk\omega} N(\xi)^3 - \frac{\omega + k}{2k^2 s\omega} N(\xi)^2 + c_1 N(\xi) \right] \mathrm{d}\xi, \\ &= \int_0^\infty \left[-\frac{N_1^2}{2} \mathrm{sech}^2(\xi) \tanh^2(\xi) + \frac{r N_1^3}{12sk\omega} \mathrm{sech}^3(\xi) + c_1 N_1 \mathrm{sech}(\xi) \right. \\ &\quad \left. - \frac{N_1^2(\omega + k)}{2sk^2\omega} \mathrm{sech}^2(\xi) \right] \mathrm{d}\xi, \\ &= N_1 \left(\frac{\pi r}{48ks\omega} N_1^2 - \left\{ \frac{1}{6} + \frac{\omega + k}{2s\omega k^2} \right\} N_1 + \frac{c_1 \pi}{2} \right). \end{aligned} \tag{26}$$

Using the Ritz-like method [48], the stationary condition for Equation (26) is

$$\frac{\mathrm{d}\mathcal{J}}{\mathrm{d}N_1} = \frac{\pi r}{16ks\omega} N_1^2 - \left\{ \frac{1}{3} + \frac{\omega + k}{s\omega k^2} \right\} N_1 + \frac{c_1 \pi}{2} = 0. \tag{27}$$

Solving (27) for N_1, we obtain

$$N_1 = \frac{2}{3\pi rk} \left[4(sk^2\omega + 3k + 3\omega) \pm \sqrt{16(k^2 s + 3)^2 \omega^2 + ((96 - 18c_1 r\pi^2)sk^3 + 288k)\omega + 144k^2} \right]. \tag{28}$$

Thus, a bright soliton solution to Equation (2) has the form

$$\begin{aligned} \mathcal{H} &= \frac{2}{3\pi rk} \left[4(sk^2\omega + 3k + 3\omega) \pm \sqrt{16(k^2 s + 3)^2 \omega^2 + ((96 - 18c_1 r\pi^2)sk^3 + 288k)\omega + 144k^2} \right] \\ &\quad \times \mathrm{sech}\left(\frac{kx^p}{\Gamma(p+1)} + \omega t \right) e^{\sigma \mathbb{B}(t) - \frac{\sigma^2}{2} t}, \end{aligned} \tag{29}$$

which is a new solution.

4.2. Bright-like Soliton

The bright-like soliton solution to Equation (2) is assumed to have the form [49]

$$N(\xi) = \frac{N_2}{1+\cosh(\xi)}, \tag{30}$$

where N_2 is a constant. Substituting the expression (30) into Equation (24) implies the following:

$$\begin{aligned}\mathcal{J} &= \int_0^\infty \left\{ \frac{rN_2^3}{12sk\omega(1+\cosh(\xi))^3} - \frac{(\omega+k)N_2^2}{2sk^2\omega(1+\cosh(\xi))^2} + \frac{c_1N_2}{1+\cosh(\xi)} \right\} \mathrm{d}\xi, \\ &= N_2\left(\frac{rN_2^2}{90sk\omega} - \frac{(\omega+k)N_2}{6sk^2\omega} + c_1 \right).\end{aligned} \tag{31}$$

The stationary condition for (31) is

$$\frac{\mathrm{d}\mathcal{J}}{\mathrm{d}N_2} = \frac{r}{30sk\omega}N_2^2 - \frac{10(k+\omega)}{30sk^2\omega}N_2 + c_1 = 0. \tag{32}$$

Solving (32) for N_2, we obtain

$$N_2 = \frac{1}{rk}\left[5(k+\omega) \pm \sqrt{25(\omega^2+k^2) + 10k(5-3c_1rsk^2)\omega} \right]. \tag{33}$$

Thus, the bright dark solution to Equation (2) has the form

$$\begin{aligned}\mathcal{H} = &\frac{1}{rk(1+\cosh(\frac{kx^p}{\Gamma(p+1))}+\omega t)} \left[5(k+\omega) \pm \sqrt{25(\omega^2+k^2) + 10k(5-3c_1rsk^2)\omega} \right] \\ &\times e^{\sigma\mathbb{B}(t)-\frac{\sigma^2}{2}t},\end{aligned} \tag{34}$$

which is new.

4.3. Kinky-Bright Soliton

To obtain the kinky-bright soliton, we assume

$$N(\xi) = N_3\mathrm{sech}^2(\xi), \tag{35}$$

where N_3 is a constant. Substituting the expression (35) into the Equation (24) yields

$$\begin{aligned}\mathcal{J} &= \int_0^\infty \left\{ -2N_3^2\mathrm{sech}^4(\xi)\tanh^2(\xi) + \frac{rN_3^3}{12sk\omega}\mathrm{sech}^6(\xi) - \frac{N_3^3(\omega+k)}{2sk^2\omega}\mathrm{sech}^4(\xi) + c_1N_3\mathrm{sech}^2(\xi) \right\} \mathrm{d}\xi, \\ &= N_3\left\{ \frac{2rN_3^2}{45sk\omega} - \left(\frac{4}{15} + \frac{\omega+k}{3sk\omega} \right) N_3 + c_1 \right\}.\end{aligned} \tag{36}$$

The stationary condition for (36) is

$$\frac{\mathrm{d}\mathcal{J}}{\mathrm{d}N_3} = \frac{2r}{15sk\omega}N_3^2 - \frac{2(4sk^2\omega+5k+5\omega}{15sk^2\omega}N_3 + c_1 = 0. \tag{37}$$

Solving (37) for N_3 gives

$$N_3 = \frac{1}{2rk}[5k+5\omega+4sk^2\omega \pm \sqrt{(4sk^2+5)^2\omega^2 + 10((4-3c_1r)sk^3+5k)\omega + 25k^2}]. \tag{38}$$

Hence, a Kinky-bright soliton solution to Equation (2) has the form

$$\begin{aligned}\mathcal{H} = \frac{1}{2rk}[5k + 5\omega + 4sk^2\omega \pm \sqrt{(4sk^2+5)^2\omega^2 + 10((4-3c_1r)sk^3 + 5k)\omega + 25k^2}] \\ \times \operatorname{sech}^2(\frac{kx^p}{\Gamma(p+1))} + \omega t)e^{\sigma\mathbb{B}(t)-\frac{\sigma^2}{2}t},\end{aligned} \tag{39}$$

which is new.

4.4. Periodic Wave Solution

To construct a periodic wave solution to Equation (2), we assume it has the form

$$N(\xi) = N_4\cos(\xi), \tag{40}$$

where N_4 is a constant. Substituting the expression (40) into Equation (24) gives

$$\mathcal{J} = \int_0^{T/4}\left\{\frac{rN_4^3}{12sk\omega}\cos^3(\xi) + \frac{N_4^2(sk^2\omega - k - \omega}{2sk^2\omega}\cos^2(\xi) + c_1N_4\cos(\xi) - \frac{N_4^2}{2}\right\}\mathrm{d}\xi, \tag{41}$$

where $T = \pi$ is the period of the nonlinear term in Equation (6). Hence, we have

$$\mathcal{J}(N_4) = N_4\left(\frac{5r\sqrt{2}}{144ks\omega}N_4^2 - \frac{s\omega(\pi-2)k^2 + (2+\pi)(\omega+k)}{16s\omega k^2}N_4 + \frac{c_1\sqrt{2}}{2}\right). \tag{42}$$

The stationary condition for Equation (42) is

$$\frac{\mathrm{d}\mathcal{J}}{\mathrm{d}N_4} = \frac{5r\sqrt{2}}{48ks\omega}N_4^2 - \frac{N_4}{8s\omega k^2}[s\omega(\pi-2)k^2 + (k+\omega)(2+\pi)] + \frac{c_1\sqrt{2}}{2} = 0. \tag{43}$$

Solving (43) for N_4, we obtain

$$\begin{aligned}N_4 = \frac{1}{10rk}[\pm\sqrt{18(s(\pi-2)k^2+\pi+2)^2\omega^2 - 480k\left(s\left(c1r - \frac{3\pi^2}{40} + \frac{3}{10}\right)k^2 - \frac{3(2+\pi)^2}{40}\right)\omega + 18k^2(2+\pi)^2} \\ + 3\Big(\Big(s\omega\,k^2 + k + \omega\Big)\pi - 2s\omega\,k^2 + 2k + 2\omega\Big)\sqrt{2}]\end{aligned} \tag{44}$$

Hence, Equation (2) has a periodic wave solution of the form

$$\begin{aligned}\mathcal{H} = \frac{1}{10rk}[\pm\sqrt{18(s(\pi-2)k^2+\pi+2)^2\omega^2 - 480k\left(s\left(c_1r - \frac{3\pi^2}{40} + \frac{3}{10}\right)k^2 - \frac{3(2+\pi)^2}{40}\right)\omega + 18k^2(2+\pi)^2} \\ + 3\Big(\Big(s\omega\,k^2 + k + \omega\Big)\pi - 2s\omega\,k^2 + 2k + 2\omega\Big)\sqrt{2}]\cos(\frac{kx^p}{\Gamma(p+1))} + \omega t)e^{\sigma\mathbb{B}(t)-\frac{\sigma^2}{2}t},\end{aligned} \tag{45}$$

which is a new solution.

5. Graphic Representation

In this section we examine how the order of the fractional derivative, p, and the noise strength, σ, influence some of the obtained solutions.

Assuming $r = 0.1703$ and $s = 0.005$, Equation (2) has the form

$$\mathrm{d}\mathcal{H} + [\mathbb{D}_x^p\mathcal{H} - 0.08515\mathcal{H}\mathbb{D}_x^p\mathcal{H}]\mathrm{d}t - 0.005\mathbb{D}_x^{2p}\mathrm{d}\mathcal{H} = \sigma(\mathcal{H} - 0.005\mathbb{D}_x^{2p}\mathcal{H})\mathrm{d}\mathbb{B}. \tag{46}$$

If we also choose $\omega = -5, k = 6, c_1 = -11.495$, and $c_2 = 9$, we obtain, using (10), that $\alpha = 1, \beta = -3$, and $\gamma = 1.5$. Thus, $\Delta = 0.4375 > 0$ and $\beta < 0$. This choice of the parameter results in a problem that falls in Case C above. The roots of the polynomial (12) are $\psi_2 = -1.942241851, \psi_3 = 0.5578746983$, and $\psi_4 = 1.384367153$, and there are two types of solutions depending on the intervals of real propagation. We restrict our discussion to the bounded solution. So, solution (19) takes the form

$$\mathcal{H}(x,t) = \left[1.391091483 + 2.500116549\,\mathrm{sn}^2\left(-\frac{0.2039181516x^p}{\Gamma(p+1)} + 0.1699317930t, 0.8669204507\right)\right] \times e^{\sigma\mathbb{B}(t)-\frac{\sigma^2}{2}t}. \quad (47)$$

Figure 1 shows a graphical representation of the solution of Equation (2) for the case where the fractional derivative order is set to one. The figure shows how the solution evolves under varying noise strengths. In Figure 1a, a 2D plot of the solution (19) reveals that the system exhibits periodic behavior when $\sigma = 0$ (the deterministic case). As the noise strength increases, the amplitude and width of the solution decrease. For higher noise levels, the periodic pattern weakens, and the solution eventually flattens, as indicated by the green curve in Figure 1a. The 3D representations in the noise-free case (Figure 1b) show a smooth and periodic surface. However, when weak noise is introduced ($\sigma > 0$), minor irregularities or undulations appear (Figure 1c), indicating slight deviations from the deterministic solution. For sufficiently large noise values, the surface becomes entirely flat as shown in Figure 1d.

Figure 2 shows the periodic solution (19) to Equation (2), for the deterministic case ($\sigma = 0$) with various fractional derivative orders p. Figure 2a shows that for $p = 1$, the solution is periodic. As the fractional derivative order decreases from one, the solution maintains nearly constant amplitude while experiencing significant width expansion. The 3D representation reveals that the solution surface (19) is smooth and periodic when $p = 1$. While periodicity persists at $p = 0.8$, the solution width increases substantially compared to Figure 2b. For smaller orders of fractional derivatives, this width expansion becomes even more pronounced.

The solutions clearly depend on the parameters Δ, β, γ, which are determined by ω, k, c_1, c_2. For our analysis, we specifically choose the following parameter values: $c_1 = -18.69503906, \omega = -6.901779743, s = 0.0001713436720$, and $k = 6$. Using these values, the expressions in (10) yield $\beta = -3, \gamma = 2, \alpha = 1$, and thus, $\Delta = 0$. As a result, the solution (14) to Equation (46) corresponds to Case A, takes the form:

$$\mathcal{H}(x,t) = \left[1.333333334 + 3\tanh^2\left(-\frac{0.1936491673x^p}{\Gamma(p+1)} + 0.1613743061t\right)\right] e^{\sigma\mathbb{B}(t)-\frac{\sigma^2}{2}t}, \quad (48)$$

which is a solitary solution. We now analyze how the solution (14) responds independently to (a) noise strength σ and (b) fractional order p.

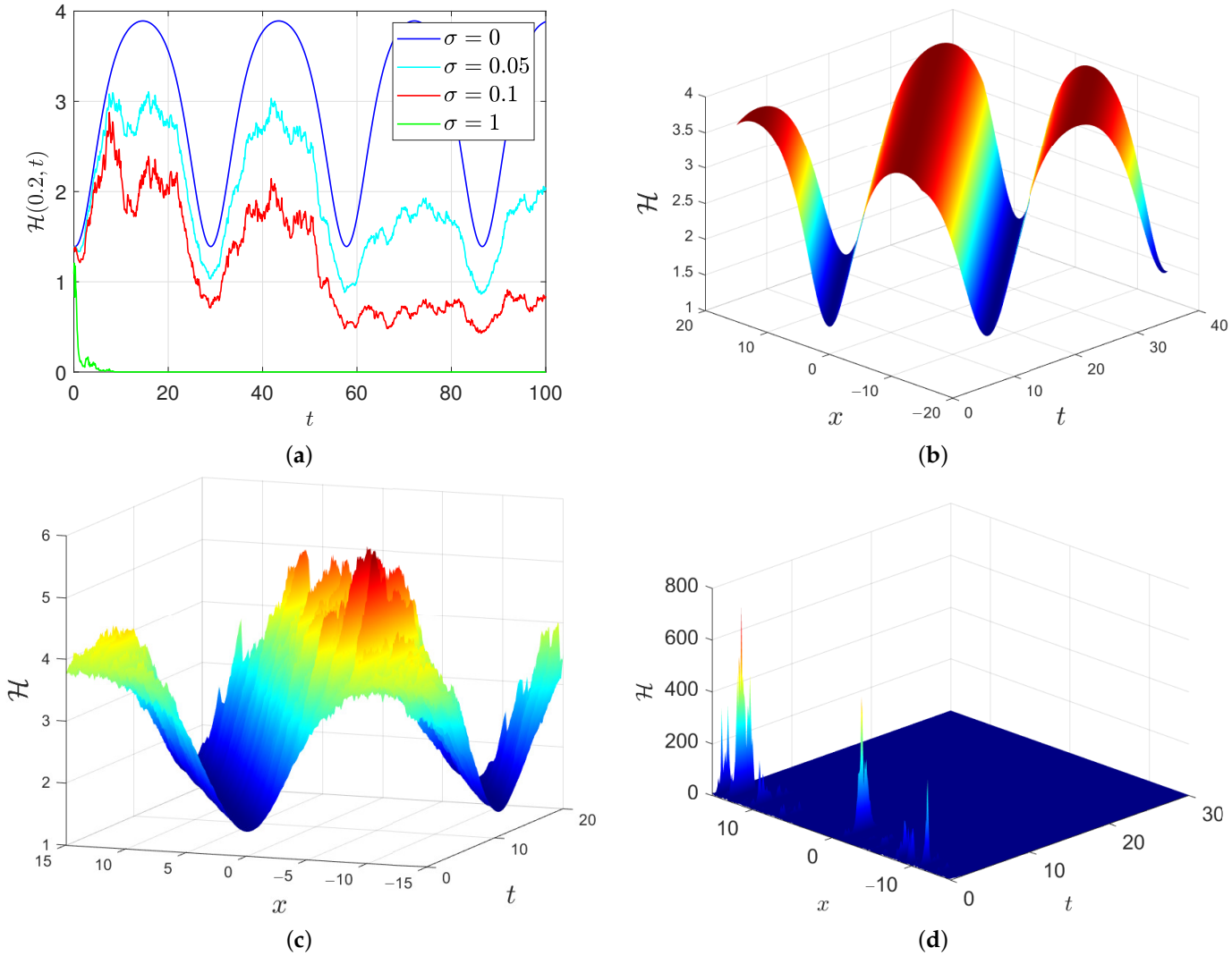


Figure 1. The graphic representation of the solution (19) when the fractional order derivative is one: (**a**) 2D representation for different values of the noise strength; (**b**) 3D representation when $\sigma = 0$; (**c**) 3D representation when $\sigma = 0.05$; (**d**) 3D representation when $\sigma = 1$.

Figure 3 shows this solution for $p = 1$ and varying σ values: in the 2D representation (Figure 3a), the deterministic case ($\sigma = 0$, blue curve) appears symmetric, but increasing σ disrupts this symmetry, initially amplifying both the solution's amplitude and width before causing decay of both at higher noise levels (green curve). The 3D evolution reveals a smooth solitary surface for $\sigma = 0$ (Figure 3b), which develops roughness under weak noise (Figure 3c) and ultimately flattens over time for large σ (Figure 3d), demonstrating noise-driven suppression of the original solution.

Figure 4 illustrates the behavior of the solution given in (14) for the noise-free case, and different values of the fractional derivative order. The 2D plot in Figure 4a reveals that as the order of the fractional derivatives decreases from unity, the solution's amplitude remains largely constant, whereas its width expands. In Figure 4b, the surface described by (14) appears smooth and solitary when $p = 1$. For values of p less than one, the surface retains its smoothness but loses symmetry due to the progressive increase in its width.

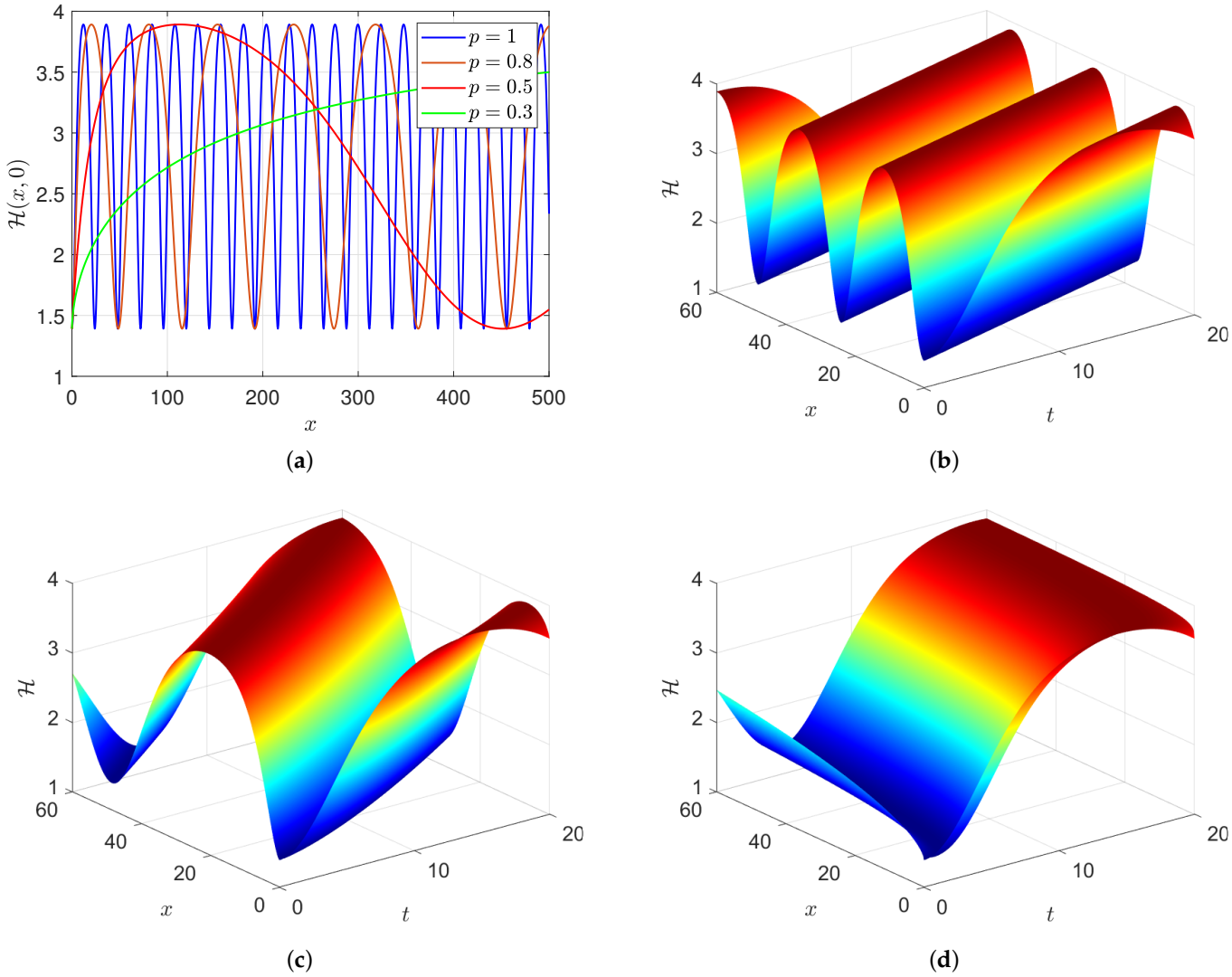


Figure 2. The graphic representation to the solution (19) in the deterministic case ($\sigma = 0$) (**a**) 2D representation for different values of the fractional order derivative (**b**) 3D representation when $p = 1$ (**c**) 3D representation when $p = 0.8$ (**d**) 3D representation when $p = 0.3$.

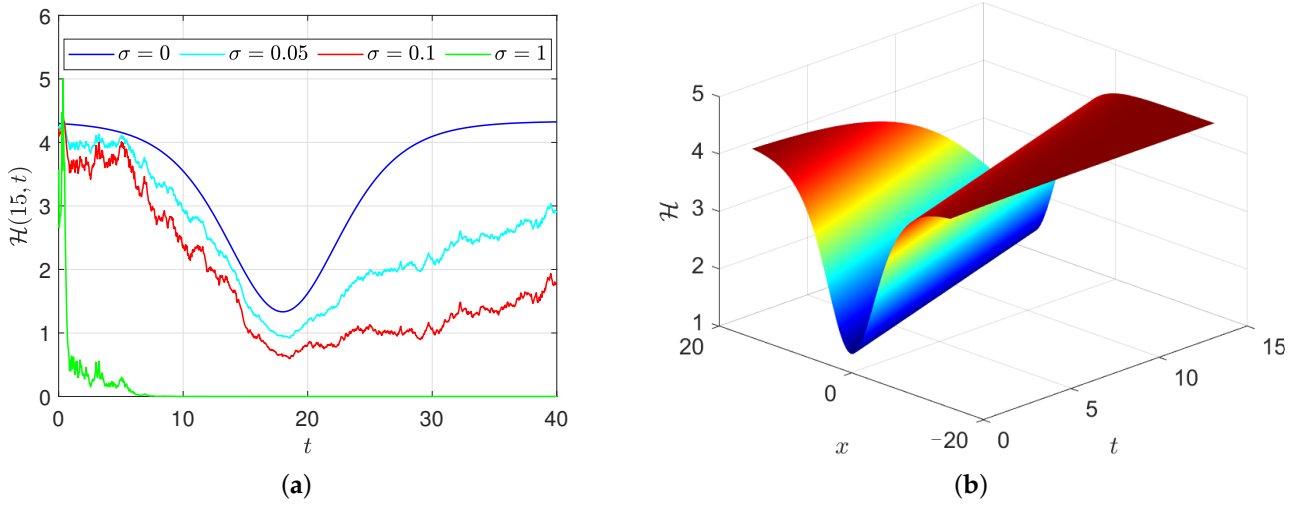
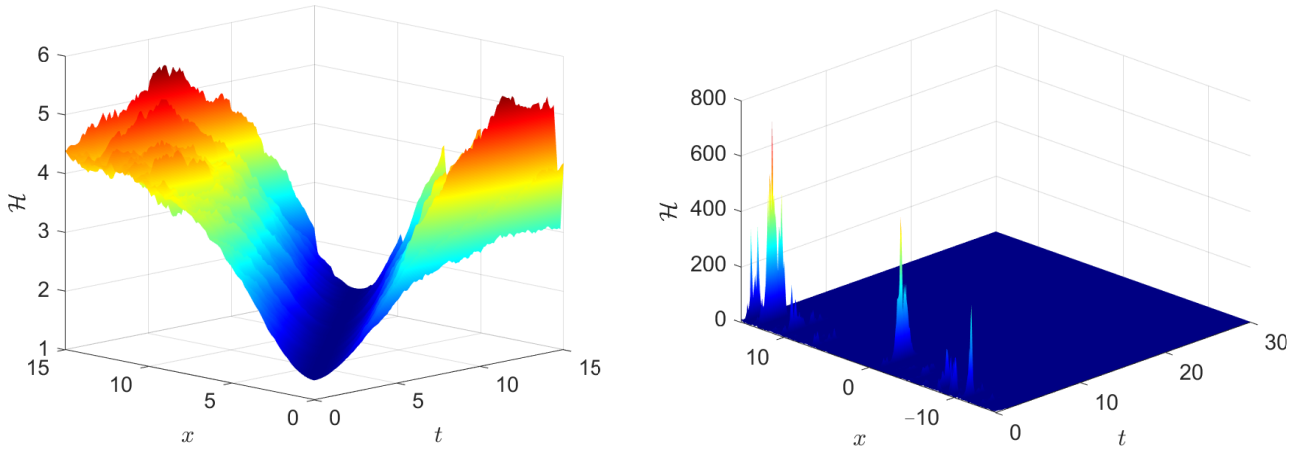
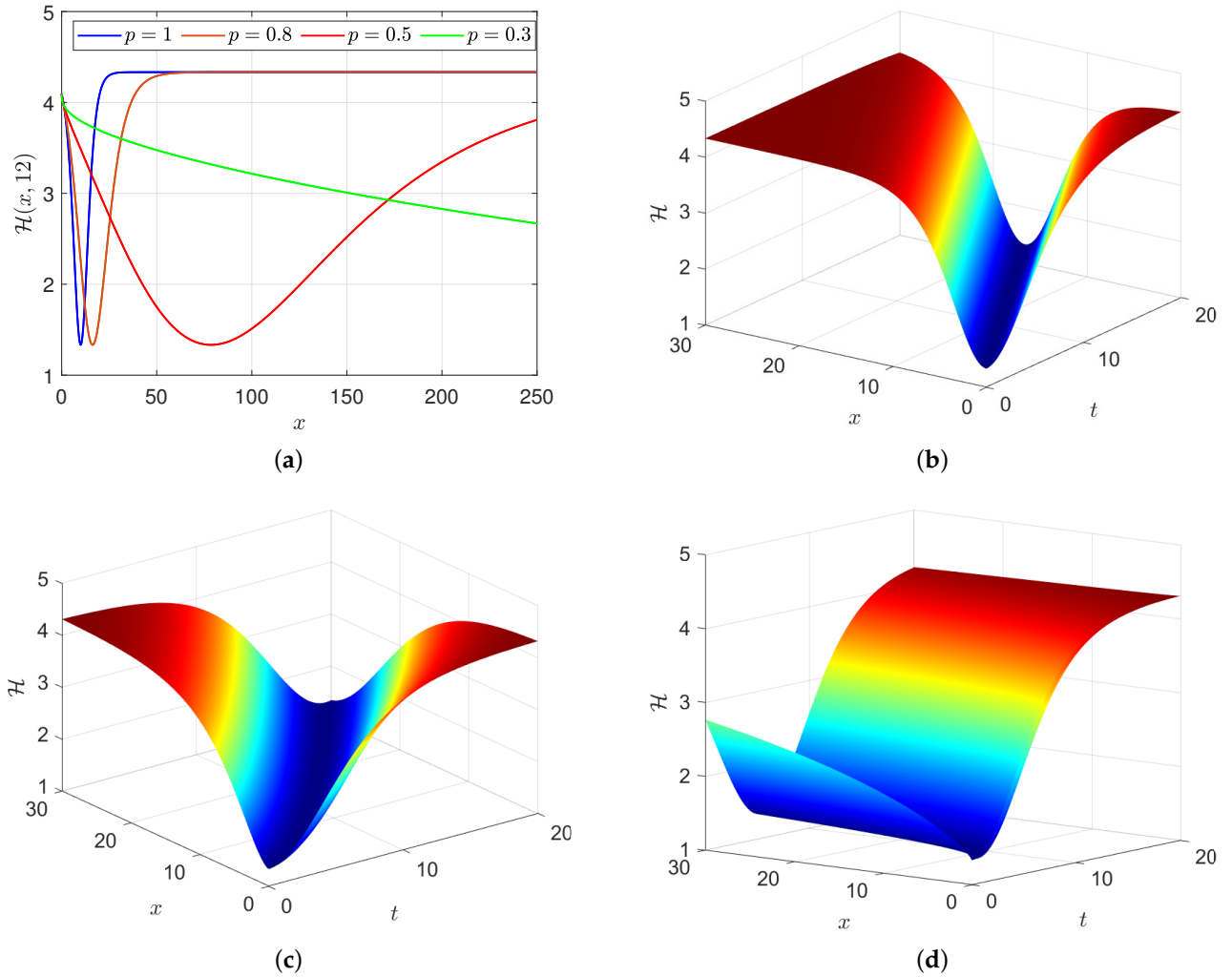


Figure 3. *Cont.*



(**c**) (**d**)

Figure 3. The graphic representation to the solution (14) when the fractional order ($p = 1$) (**a**) 2D representation for different values of the noise strength (**b**) 3D representation when $\sigma = 0$ (**c**) 3D representation when $\sigma = 0.05$ (**d**) 3D representation when $\sigma = 2$.



(**a**) (**b**)

(**c**) (**d**)

Figure 4. The graphic representation to the solution (14) in the deterministic case ($\sigma = 0$) (**a**) 2D representation for different values of the fractional order p (**b**) 3D representation when $p = 1$ (**c**) 3D representation when $p = 0.8$ (**d**) 3D representation when $p = 0.4$.

6. Conclusions

This study examines the influence of multiplicative noise, characterized by a Wiener process, and the fractional derivative order in the sense of Jumarie's modified Riemann–Liouville definition on the solution of the fractional stochastic regularized long wave(SFRLW) equation. A suitable wave transformation is applied to convert the SFRLW equation into an equivalent ordinary differential equation. The resulting equation is solved using two distinct approaches. The first approach, the complete discriminant polynomial system, determines the range of physical parameters necessary for integrating both sides of Equation (11). As was shown in the paper, intervals of real solutions can be used to distinguish between solutions that have very different mathematical properties. These intervals were used to construct real solutions for Equation (2), leading to novel solutions. The variational principle was employed to obtain further solutions to Equation (2), which are classified as bright solitons, bright-like solitons, kinky bright solitons, and periodic solutions. Two types of solutions—periodic and solitary— were depicted graphically to demonstrate the effects of fractional-order derivatives and noise strength on the solutions. This was achieved by starting with the deterministic case and varying the fractional derivative order. We also examine the effect of varying noise for the nonfractional case. These effects were reflected in key solution properties, including amplitude, width, and smoothness. Finally, while our study focuses on analytical solutions for the space-fractional stochastic RLW equation, the results have implications for wave phenomena such as tsunamis, internal waves, and coastal dynamics. The inclusion of stochasticity accounts for real-world uncertainties (e.g., variable topography, atmospheric forcing), which is critical for applications like tsunami prediction. Although it is not an operational tool, our framework provides theoretical foundations for future applied models.

Author Contributions: Conceptualization, M.A.N. and A.A.; Methodology, M.A.N. and B. A. and A.A.; Software, A.A.; Formal analysis, B.A. and M.A.N.; Writing—Original Draft, M.A.N. and B.A.; Writing—Review and Editing, B.A. and A.A.; Visualization, B.A.; Supervision, M.A.N. and A.A. All authors have read and agreed to the published version of the manuscript.

Funding: This work was supported by the Deanship of Scientific Research, Vice Presidency for Graduate Studies and Scientific Research, King Faisal University, Saudi Arabia [Grant No. KFU252274].

Data Availability Statement: All relevant data are within the manuscript.

Acknowledgments: The authors acknowledge the Deanship of Scientific Research at King Faisal University for the financial support.

Conflicts of Interest: The authors declare no conflicts of interest.

References

1. Hirsch, M.W.; Smale, S.; Devaney, R.L. *Differential Equations, Dynamical Systems, and an Introduction to Chaos*; Academic Press: Cambridge, MA, USA; Elsevier: Amsterdam, The Netherlands, 2013. [CrossRef]
2. Farlow, S. *Partial Differential Equations for Scientists and Engineers*; Dover Publications: Mineola, NY, USA, 1993. [CrossRef]
3. Evans, L.C. *An Introduction to Stochastic Differential Equations*; American Mathematical Society: Providence, RI, USA, 2013.
4. Platen, E.; Bruti-Liberati, N. *Numerical Solution of Stochastic Differential Equations with Jumps in Finance*; Springer Science & Business Media: Berlin/Heidelberg, Germany, 2010; Volume 64.
5. Braumann, C.A. *Introduction to Stochastic Differential Equations with Applications to Modelling in Biology and Finance*; Wiley: Hoboken, NJ, USA, 2019. [CrossRef]
6. Kamrani, M. Numerical solution of stochastic fractional differential equations. *J. Fluid Mech.* **2015**, *68*, 81–93. [CrossRef]
7. Ha, T.; Li, Z.; Kun, K. Exact solutions of the stochastic fractional long–short wave interaction system with multiplicative noise in generalized elastic medium. *Results Phys.* **2023**, *44*, 106174. [CrossRef]
8. AL Nuwairan, M. Bifurcation and Analytical Solutions of the Space-Fractional Stochastic Schrödinger Equation with White Noise. *Fractal Fract.* **2023**, *7*, 157. [CrossRef]

9. Yang, M. Existence uniqueness of mild solutions for Ψ-Caputo fractional stochastic evolution equations driven by fBm. *J. Inequal. Appl.* **2021**, *2021*, 170. [CrossRef]
10. Yuan, C.; Mao, X. Convergence of the Euler–Maruyama method for stochastic differential equations with Markovian switching. *Math. Comput. Simul.* **2004**, *64*, 223–235. [CrossRef]
11. Elbrolosy, M.; Alhamud, M.; Elmandouh, A. Analytical solutions to the fractional stochastic (3 + 1) equation of fluids with gas bubbles using an extended auxiliary function method. *Alex. Eng. J.* **2024**, *92*, 254–266. [CrossRef]
12. Mohammed, W.W.; Cesarano, C.; Elmandouh, A.A.; Alqsair, I.; Sidaoui, R.; Alshammari, H.W. Abundant optical soliton solutions for the stochastic fractional fokas system using bifurcation analysis. *Phys. Scr.* **2024**, *99*, 045233. [CrossRef]
13. Li, S.; Khan, S.; Riaz, M.; AlQahtani, S.A.; Alamri, M.M. Numerical simulation of a fractional stochastic delay differential equations using spectral scheme: A comprehensive stability analysis. *Sci. Rep.* **2024**, *14*, 6930. [CrossRef]
14. Moghaddam, B.P.; Babaei, A.; Dabiri, A.; Galhano, A. Fractional Stochastic Partial Differential Equations: Numerical Advances and Practical Applications—A State of the Art Review. *Symmetry* **2024**, *16*, 563. [CrossRef]
15. Peregrine, D.H. Calculations of the development of an undular bore. *J. Fluid Mech.* **1966**, *25*, 321–330. [CrossRef]
16. Benjamin, T.B.; Bona, J.L.; Mahony, J.J. Model equations for long waves in nonlinear dispersive systems. *Philos. Trans. R. Soc. Lond. Ser. A Math. Phys. Sci.* **1972**, *272*, 47–78. [CrossRef]
17. Bona, J.L.; Bryant, P.J. A mathematical model for long waves generated by wavemakers in non-linear dispersive systems. *Math. Proc. Camb. Philos. Soc.* **1973**, *73*, 391–405. [CrossRef]
18. Eilbeck, J.; McGuire, G. Numerical study of the regularized long-wave equation I: Numerical methods. *J. Comput. Phys.* **1975**, *19*, 43–57. [CrossRef]
19. El-Danaf, T.S.; Ramadan, M.A.; Abd Alaal, F.E. The use of adomian decomposition method for solving the regularized long-wave equation. *Chaos Solitons Fractals* **2005**, *26*, 747–757. [CrossRef]
20. Pshtiwan, O.M.; Alqudah, M.A.; Hamed, Y.S.; Kashuri, A.; Abualnaja, K.M. Solving the Modified Regularized Long Wave Equations via Higher Degree B-Spline Algorithm. *J. Funct. Spaces* **2021**, *2021*, 5580687. [CrossRef]
21. Maarouf, N.; Maadan, H.; Hilal, K. Lie symmetry analysis and explicit solutions for the time-fractional regularized long-wave equation. *Int. J. Differ. Equ.* **2021**, *2021*, 6614231. [CrossRef]
22. Kumar, D.; Singh, J.; Baleanu, D.; Sushila. Analysis of regularized long-wave equation associated with a new fractional operator with Mittag-Leffler type kernel. *Phys. A Stat. Mech. Its Appl.* **2018**, *492*, 155–167. [CrossRef]
23. Jhangeer, A.; Muddassar, M. andKousar, M.; Infal, B. Multistability and Dynamics of Fractional Regularized Long Wave equation with Conformable Fractional Derivatives. *Ain Shams Eng. J.* **2021**, *12*, 2153–2169. [CrossRef]
24. Jumarie, G. Modified Riemann-Liouville derivative and fractional Taylor series of nondifferentiable functions further results. *Comput. Math. Appl.* **2006**, *51*, 1367–1376. [CrossRef]
25. Calin, O. *An Informal Introduction to Stochastic Calculus with Applications*; World Scientific: Singapore, 2015.
26. Al-Askar, F.M.; Cesarano, C.; Mohammed, W.W. Effects of the wiener process and beta derivative on the exact solutions of the kadomtsev–petviashvili equation. *Axioms* **2023**, *12*, 748. [CrossRef]
27. Mohammed, W.W.; Alshammari, M.; Cesarano, C.; Albadrani, S.; El-Morshedy, M. Brownian motion effects on the stabilization of stochastic solutions to fractional diffusion equations with polynomials. *Mathematics* **2022**, *10*, 1458. [CrossRef]
28. Almutairi, B.; Al Nuwairan, M.; Aldhafeeri, A. Exploring the Exact Solution of the Space-Fractional Stochastic Regularized Long Wave Equation: A Bifurcation Approach. *Fractal Fract.* **2024**, *8*, 298. [CrossRef]
29. Al Nuwairan, M.; Elmandouh, A. Modification to an Auxiliary Function Method for Solving Space-Fractional Stochastic Regularized Long-Wave Equation. *Fractal Fract.* **2025**, *9*, 298. [CrossRef]
30. Pandit, S. A new algorithm for analysis and simulation of (2 + 1) Korteweg–de Vries–Rosenau-regularized long-wave model. *Comput. Appl. Math.* **2024**, *43*, 35. [CrossRef]
31. Pandit, S. Local radial basis functions and scale-3 Haar wavelets operational matrices based numerical algorithms for generalized regularized long wave model. *Wave Motion* **2022**, *109*, 102846. [CrossRef]
32. Kumar, S.; Jiwari, R.; Mittal, R.; Awrejcewicz, J. Dark and bright soliton solutions and computational modeling of nonlinear regularized long wave model. *Nonlinear Dyn.* **2021**, *104*, 661–682. [CrossRef]
33. Peregrine, D.H. Long waves on a beach. *J. Fluid Mech.* **1967**, *27*, 815–827. [CrossRef]
34. Shi, F.; Kirby, J.T.; Harris, J.C.; Geiman, J.D.; Grilli, S.T. A high-order adaptive time-stepping TVD solver for Boussinesq modeling of breaking waves and coastal inundation. *Ocean Model.* **2012**, *43*, 36–51. [CrossRef]
35. Chazel, F.; Benoit, M.; Ern, A.; Piperno, S. A double-layer Boussinesq-type model for highly nonlinear and dispersive waves. *Proc. R. Soc. A Math. Phys. Eng. Sci.* **2009**, *465*, 2319–2346. [CrossRef]
36. Popinet, S. A vertically-Lagrangian, non-hydrostatic, multilayer model for multiscale free-surface flows. *J. Comput. Phys.* **2020**, *418*, 109609. [CrossRef]
37. Yang, L.; Hou, X.; Zeng, Z. A complete discrimination system for polynomials. *Sci. China Ser. E* **1996**, *39*, 628–646.

38. He, J.H. Asymptotic methods for solitary solutions and compactons. In *Proceedings of the Abstract and Applied Analysis*; Wiley Online Library: Hoboken, NJ, USA, 2012; Volume 2012, p. 916793.
39. Kilbas, A.A.; Srivastava, H.M.; Trujillo, J.J. *Theory and Applications of Fractional Differential Equations*; Elsevier: Amsterdam, The Netherlands, 2006.
40. AL Nuwairan, M. The exact solutions of the conformable time fractional version of the generalized Pochhammer–Chree equation. *Math. Sci.* **2023**, *17*, 305–316. [CrossRef]
41. Byrd, P.F.; Friedman, M.D. *Handbook of Elliptic Integrals for Engineers and Scientists*, 2nd ed.; Die Grundlehren der Mathematischen Wissenschaften, Band 67; Springer: New York, NY, USA; Berlin/Heidelberg, Germany, 1971.
42. He, J.H. Semi-inverse method of establishing generalized variational principles for fluid mechanics with emphasis on turbomachinery aerodynamics. *Int. J. Turbo Jet Engines* **1997**, *14*, 23–28. [CrossRef]
43. He, J.H.; Sun, C. A variational principle for a thin film equation. *J. Math. Chem.* **2019**, *57*, 2075–2081. [CrossRef]
44. He, J.H.; García, A. The simplest amplitude-period formula for non-conservative oscillators. *Rep. Mech. Eng.* **2021**, *2*, 143–148. [CrossRef]
45. He, J.H.; Qie, N.; He, C.H.; Saeed, T. On a strong minimum condition of a fractal variational principle. *Appl. Math. Lett.* **2021**, *119*, 107199. [CrossRef]
46. He, J.H.; Qie, N.; He, C.H. Solitary waves travelling along an unsmooth boundary. *Results Phys.* **2021**, *24*, 104104. [CrossRef]
47. He, J.H.; Hou, W.F.; He, C.H.; Saeed, T.; Hayat, T. Variational approach to fractal solitary waves. *Fractals* **2021**, *29*, 2150199. [CrossRef]
48. Elboree, M.K. Soliton solutions for some nonlinear partial differential equations in mathematical physics using He's variational method. *Int. J. Nonlinear Sci. Numer. Simul.* **2020**, *21*, 147–158. [CrossRef]
49. Wang, K.J.; Wang, G.D. Variational theory and new abundant solutions to the (1 + 2)-dimensional chiral nonlinear Schrödinger equation in optics. *Phys. Lett. A* **2021**, *412*, 127588. [CrossRef]

Disclaimer/Publisher's Note: The statements, opinions and data contained in all publications are solely those of the individual author(s) and contributor(s) and not of MDPI and/or the editor(s). MDPI and/or the editor(s) disclaim responsibility for any injury to people or property resulting from any ideas, methods, instructions or products referred to in the content.